Grey-box Modelling of a Household Refrigeration Unit Using Time Series Data in Application to Demand Side Management

Fabrizio Sossan[a,*], Venkatachalam Lakshmanan[a], Giuseppe Tommaso Costanzo[a], Mattia Marinelli[a], Philip J. Douglass[a], Henrik Bindner[a]

[a]*DTU Elektro, Frederiksborgvej 399, 4000, Roskilde, Denmark*

Abstract

This paper describes the application of stochastic grey box modelling to identify electrical power consumption-to-temperature models of a domestic freezer using experimental measurements. The models are formulated using stochastic differential equations (SDEs), estimated by maximum likelihood estimation (MLE), validated through the model residuals analysis and cross-validated to detect model over-fitting. A nonlinear model based on the reversed Carnot cycle is also presented and included in the modelling performance analysis. As an application of the models, we apply model predictive control (MPC) to shift the electricity consumption of a freezer in demand response experiments, thereby addressing the model selection problem also from the application point of view and showing in an experimental context the ability of MPC to exploit the freezer as a demand side resource (DSR).

Keywords: Power demand, Modelling, Refrigerators, Smart grids, Demand Response.

1. Introduction

Household refrigerators account for a noticeable share of the total residential electricity demand (e.g. 7% in the US [1]) and are gaining attention in the context of demand side management (DSM) [2–4]. Validated mathematical models and procedures for on-line system identification of refrigeration units are of importance for assessing their energy efficiency, predicting their power consumption and in application to intelligent energy management strategies to support power system operation, such as model predictive control (MPC) [5, 6]. In the first part of this paper, we describe the application of a state-of-the-art grey-box modelling methodology to identify power consumption-to-temperature prediction models using experimental measurements from a conventional domestic freezer. The modelling effort aims to identify the model structure and parameters of the physical processes associated with the operation of the freezer, i.e. heat transfer and refrigeration cycle coefficient

of performance (COP). Consumer behavior modelling is not considered at this stage. In the second part of the paper, the proposed models are used to implement a MPC strategy in order to experimentally achieve a shift in the energy consumption of the freezer. The contribution of this paper is twofold. First, novel validated grey-box models for a domestic freezer are proposed. Existing models in the literature were mainly developed using first principle approaches (see for example [7–9]). So-called white-box models in application to demand side management do not allow to achieve any degree of differentiation when dealing with different units. This property does not make them suitable for future smart grid scenarios, where demand response built up from the contribution of heterogeneous populations of demand side resources (DSRs) is expected to play a central role in assuring reliable power system operation. On the contrary, grey-box models are adaptive by nature since they are estimated from measurements and potentially allow for tracking system changes on-line by reiterating the estimation procedure. A set of linear grey-box models for a domestic fridge was proposed in [10]. In this case, we extend the already existing liter-

---

*Corresponding author
Email address: `fabrizio.sossan@epfl.ch` (Fabrizio Sossan)

ature by considering a domestic freezer and, especially, by including in the modelling performance assessment a nonlinear grey-box model based on the reversed Carnot cycle. Second, by implementing the consumption shift experiments in a real operating environment, we address the model selection problem from the specific perspective of the application, that is finally among the most relevant problems for DSM. Overall, we therefore provide a global assessment of grey-box modelling for refrigeration units analyzing both the pure modelling performance and application. The structure of the paper is as follows. Section 2 describes the experimental setup adopted for the model identification and consumption shift experiments. Section 3 describes the grey-box modelling framework adopted to identify the freezer models, which are therefore presented in Section 4. In Section 6, we perform an empirical evaluation of the thermal properties of the considered freezer with the objective of supporting grey-box modelling results. In Section 4, the models prediction performance are further assessed using validation data sets. Finally, in Section 7 a number of the proposed model are used in an MPC experiments with the objective of shifting the consumption of a freezer in the context of intelligent energy strategies for demand response applications.

2. Experimental setup

The experimental setup consists of a freezer equipped with temperature sensors, a power consumption measurements board and an external relay. The objective of the experiment is to collect the measurements for identifying the freezer models and to perform the energy shift experiments. The instrumented freezer (shown in Fig. 1) is a Bosch GSN40A21[1], a commercially available domestic unit with 333 L capacity and a single-phase compressor. During experiments, the freezer was empty and with closed door. Temperatures are measured using 10k NTC thermistors, which can measure temperatures in the range -30 to 80°C with an accuracy of $\pm 0.2\,^{\circ}$C at 25°C and have a fast measurements response. Thermistors are connected to a 12bit ADC through a resistance-to-voltage transducer. A total of 3 thermistors are used, 2 for

measuring the freezer interior temperature at different heights and one for the room temperature. The freezer power consumption is measured using a DEIF MIC-2. This accuracy class 0.5 instrument is able to measure voltages and currents up to $400\,\text{V}/5\,\text{A}$ of magnitude on a three phases bus, although only one phase is used for this application. The controllable power plug determines the state (on-off) of the freezer. In order to override the internal action of the freezer thermostat, the thermostatic set-point is set to the lowest value, and the temperature of the freezer is allowed to vary only above this threshold. In this way, the activation of the freezer compressor depends only on the state of the external relay. All the sensors and instruments are connected to a PC and are accessed by a JAVA software application. Measurements and actuations are sampled at 1 second.

Figure 1: The 333 liters domestic freezer used for the identification and MPC experiments.

3. The grey-box modelling methodology

Grey-box modelling is a framework to identify and validate a mathematical model of a system in-

---

corporating its physical knowledge together with measurements from a real device. It consists of a number of steps, which are explained in the following.

3.1. Experimental design

A control signal commonly used for model identification is the PRBS (pseudo binary random signal), an on-off signal with fixed period and uniformly distributed random duty cycle that is able to excite the system to model in a wide range of frequencies. For identifying the freezer thermal models, a PRBS was used to set the state of the controllable power plug. To avoid damaging the freezer compressor, the PRBS cycles with on-to-off transitions shorter than 30 seconds were disregarded. By doing this, it was not possible to observe very short transients, which however are of limited interest since we target to capture the dominant system dynamics. Fig. 2 shows the set of measurements used for the model identification. In the upper panel plot, it is evident the effect of the PRBS on the freezer power consumption, that is characterized by activation cycles of random length. The time series are of appropriate duration for the purpose of thermal models identification as they are considerably longer than the slowest time constant of the system (≈ 4 hours[2]). Two additional sets of measurements were collected to assess the models prediction performance (Section 6).

3.2. Measurements post-processing

The measured physical quantities are the freezer and room temperatures and freezer total power consumption. Two freezer temperature sensors are available, and their readings are averaged in order to obtain a single temperature measurements time series. Power consumption measurements were treated to remove the components not playing a role in the refrigeration cycle since they can interfere with the estimation of the model parameters. First, the power absorption of auxiliary components (like the control logic and digital display), considered constant, was removed by subtracting. Second, the power consumption spikes due to the inrush current of the induction motor driving the compressor were filtered out. The spikes usually
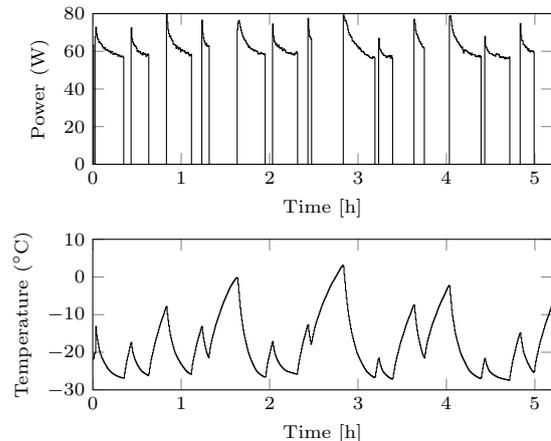

Figure 2: The measurements used to identify the freezer thermal models: the freezer power consumption under PRBS regime (upper panel) and temperature (lower panel).

extinguish in a few seconds and are disregarded because they represent the energy spent to accelerate the compressor and have a negligible impact on the thermodynamic transformation operated by the freezer.

3.3. Model Formulation

A set of mathematical relationships to describe the physical process to model is formulated. In general, refrigeration units, like freezers and fridges, implement a thermodynamic cycle to accomplish heat transfer from a cold to a hot reservoir by supplying mechanical work to the system. The freezer models are derived using the thermal equivalent circuit (TEC) approach, that considers the temperatures and heat fluxes of a thermal system as voltages and currents of an electric circuit. The proposed models as well as the basic thermodynamic concepts adopted to derive them are detailed in the following section. The models are formulated using stochastic differential equations (SDEs) and continuous time state space representation. In the linear case, the models are:

$$d\boldsymbol{x}_t = A(\boldsymbol{\theta})\boldsymbol{x}_t dt + B(\boldsymbol{\theta})\boldsymbol{u}_t dt + W(\boldsymbol{\theta})d\boldsymbol{\omega} \qquad (1)$$

$$T_k = C\boldsymbol{x}_k + v(\boldsymbol{\theta})e_k \qquad (2)$$

with $\boldsymbol{x} \in \mathbb{R}^n$ as the state vector, $\boldsymbol{u} \in \mathbb{R}^p$ input vector, $A \in \mathbb{R}^{n \times n}$ system matrix, $B \in \mathbb{R}^{n \times p}$ input matrix, $\boldsymbol{\theta} \in \mathbb{R}^m$ a vector of m model parameters, $W \in \mathbb{R}^{n \times n}$ process noise matrix (diagonal), T the estimated freezer temperature, $C \in \mathbb{R}^{1 \times n}$ output vector, $V \in \mathbb{R}$ measurement noise, and where the

---

[2]Approximatively estimated prior the model identification as 1/5 of the zero-input temperature transient duration.

subscripts t and k respectively denote continuous and discrete time quantities. The vector $\boldsymbol{\omega}$ is a standard n-dimension Wiener process, i.e. a continuous time stochastic process with independent normally distributed increment, while e_k is normal Gaussian noise. Eq. (1) describes the stochastic evolution of the system, while (2) is the observation equation and links the model state to the estimated freezer temperature.

3.4. Maximum likelihood estimation of the parameters

The parameters of the candidate model are estimated utilizing CTSM, a system identification software library for R that implements maximum likelihood estimation (MLE) [11]. In the following, a general insight on the method is given. For a comprehensive description into the algorithm, the reader is referred to [12], and to [13] for an alternative modelling application. Given a model in the form as in (1)-(2), the objective of MLE is to determine the unknown parameters $\boldsymbol{\theta}$ by maximizing the likelihood of the model getting the observed training data set. Given a time series of the output variable (such as the freezer temperature) denoted as $\mathcal{Y}_N = \{y_0, \ldots, y_N\}$, the model likelihood function is derived starting from the joint probability density:

$$L(\boldsymbol{\theta}, \mathcal{Y}_N) = p\left(\mathcal{Y}_N | \boldsymbol{\theta}\right), \tag{3}$$

that can be reformulated as a product of conditional probability densities, like

$$L(\boldsymbol{\theta}, \mathcal{Y}_N) = \left(\prod_{k=1}^{N} p(y_k | \mathcal{Y}_{k-1}, \boldsymbol{\theta})\right) p(y_0 | \boldsymbol{\theta}), \tag{4}$$

by applying the chain rule. The output of the stochastic model is completely characterized in terms of mean and variance, which are respectively given as:

$$\begin{aligned} \hat{y}_{k|k-1} &= E\left[y_k | \mathcal{Y}_{k-1}, \boldsymbol{\theta}\right] \\ R_{k|k-1} &= V\left[y_k | \mathcal{Y}_{k-1}, \boldsymbol{\theta}\right]. \end{aligned} \tag{5}$$

The one step ahead prediction errors of the model, or model residuals, are defined as the following scalar sequence:

$$\epsilon_k = y_k - \hat{y}_{k|k-1}, \quad k = 1, \ldots, N, \tag{6}$$

and the model likelihood function can be reformulated as

$$L(\boldsymbol{\theta}, \mathcal{Y}_N) = \left(\prod_{j=1}^{k} \frac{\exp\left(\frac{1}{2} \epsilon_j^2 R_{j|j-1}^{-1}\right)}{\sqrt{2\pi R_{j|j-1}}}\right) p(y_0 | \boldsymbol{\theta}), \tag{7}$$

where the formulation of the zero-mean univariate Gaussian distribution has been used. The model parameters are finally found by CTSM through minimizing the negative logarithm of the likelihood function:

$$\boldsymbol{\theta}^o = \underset{\boldsymbol{\theta} \in \Theta}{\arg \min} \; -\mathcal{L}(\boldsymbol{\theta}, \mathcal{Y}_N). \tag{8}$$

where

$$\mathcal{L}(\boldsymbol{\theta}, \mathcal{Y}_N) = \ln(L(\boldsymbol{\theta}, \mathcal{Y}_N)) \tag{9}$$

is said model log-likelihood.

3.5. Model validation through the residuals analysis

This phase consists in evaluating if the freshly identified model was able to capture all the time dynamics contained in the measurements. The model validation is carried out with the residuals analysis, that consists in evaluating any correlation in time of the model residuals (defined in (6)): if a model is acceptable, the model residuals should not show any autocorrelation or, in other words, the model explains all the dynamics in the measurements. A practical example of model validation is presented in the next section.

3.6. Model extension and cross validation

If the validation results are not satisfactory, an alternative model should be formulated by, for example, increasing the order of the previous model or adopting an alternative mathematical description of the process. The extended model parameters should be estimated and validated by reiterating the steps described in the last two paragraphs. If the model extension consisted in augmenting the model order, the following procedure is applied to test the hypothesis that the model extension is valid [14]. Given the models A and B respectively with parameters $\boldsymbol{\theta} \in \Omega_A \subset \mathbb{R}^m$ and $\boldsymbol{\theta} \in \Omega_B \subset \mathbb{R}^n$ (m and n number of parameters, $m < n$), and with $\Omega_A \subset \Omega_B$ (in other words, the simpler model is contained in the second), we test the null hypothesis $\mathcal{H}_0 : \boldsymbol{\theta} \in \Omega_A$ against the alternative $\mathcal{H}_1 : \boldsymbol{\theta} \in \Omega_B$.

The deviance (or likelihood-ratio) for the current model extension is defined as:

$$D = 2\left(\mathcal{L}(\boldsymbol{\theta} \in \Omega_B, \mathcal{Y}_N) - \mathcal{L}(\boldsymbol{\theta} \in \Omega_A, \mathcal{Y}_N)\right) \quad (10)$$

where $\mathcal{L}$ is the model log-likelihood as defined in (9). The Wilk's theorem states that, under the null hypothesis $\mathcal{H}_0$, the deviance (10) converges in law to a chi-squared distribution with $k-m$ degree of freedom (denoted by $\chi^2(k-m)$-distribution). Plainly from (10), a large deviance is in favor of the extended model. We use Wilk's theorem to define an upper threshold above which the deviance is not likely to be drawn from the $\chi^2(k-m)$-distribution, indeed giving evidence against the null hypothesis. More specifically, $\mathcal{H}_0$ is rejected at α confidence level (usually 95%) if the following condition is verified:

$$D > \Phi_{k-m}^{-1}(\alpha), \quad (11)$$

where Φ_{k-m}^{-1} is the inverse CDF of the $\chi^2(k-m)$-distribution. Equivalently, we can look at the probability of a new realization (of known distribution under $\mathcal{H}_0$) being larger than the current D, i.e.

$$p = \Pr(x > D), \quad x \in \chi^2(k-m) \quad (12)$$

that can be reformulated as:

$$\begin{aligned} p &= 1 - \Pr(x < D) \\ &= 1 - \Phi_{k-m}(D). \end{aligned} \quad (13)$$

where $\Phi_{k-m}(D)$ is the CDF of the $\chi^2(k-m)$-distribution calculated in D and can be determined, for example, using the Matlab command chi2cdf$(D, k-m)$. In (13), p is said to be the p-value. If the p-value is smaller than $1-\alpha$ (5%), the null hypothesis $\mathcal{H}_0$ is rejected and the model extension is considered valid. This procedure acts as a stop condition of the model extension process. In fact, an extended model usually performs better than the original because have a larger number of parameters, but it should be disregarded if the null hypothesis is failed to reject. A practical example of the application of this method will be provided in Section 4 when cross validating the models.

4. Freezer thermal models

In this section, the identified freezer models are presented in increasing order of complexity. As explained in the previous section, models are derived using the TEC analogy, formulated using stochastic state space representation, estimated by MLE, validated through the model residuals analysis and, in case of model extensions, cross-validated to detect model overfitting. For each model, the mathematical formulation is presented, while the estimated parameters of all the models are summarized in Appendix A.

4.1. Model A (linear first order)
4.1.1. Model formulation

Fig. 3 shows the TEC of Model A. The current Q represents the heat that is extracted from the freezer interior. In this and following linear models, Q is modelled as a function of the measured freezer power consumption P according to the following relationship:

$$Q = P \cdot \text{COP}, \quad (14)$$

where COP denotes the coefficient of performance of the refrigeration cycle, a dimensionless quantity that expresses the amount of heat transferred from the cold to the hot heat reservoir per unit of mechanical work supplied to the cycle. It is worth to note that, in the expression above, the mechanical work is approximated with the electrical power consumption. Therefore in (14), the COP coefficient should be regarded as a lumped gain that describes the coefficient of performance while accounting for power conversion losses. The capacitor C_a represents the global heat capacity of the freezer thermal mass (i.e. air content, heat exchanger and freezer envelope) and V_a corresponds to the measured freezer temperature. The electrical current flowing through the resistance R_w represents the heat losses through the freezer envelope towards the environment, that is at the room temperature T_r. The Kirchoff's voltage law (KVL) applied to the circuit in Fig. 3 constitutes the deterministic skeleton of Model A. With reference to the stochastic state space representation (1)-(2) introduced in Section 3.3, the model state and input vector are as:

$$\begin{aligned} \boldsymbol{x}^T &= V_a \\ \boldsymbol{u}^T &= \begin{bmatrix} T_r & P \end{bmatrix}, \end{aligned} \quad (15)$$

where T_r and P are the room temperature and freezer power consumption from measurements. The stochastic system matrices are:

$$A = -\frac{1}{C_a R_w} \quad (16)$$

5

$$B = \begin{bmatrix} \frac{1}{C_a R_w} & -\frac{\text{COP}}{C_a} \end{bmatrix} \quad (17)$$

$$W = w \quad (18)$$

$$C = 1 \quad (19)$$

where C_a, R_w, COP and w are the model parameters to be estimated. Their MLE-estimated values are in Table A.6.
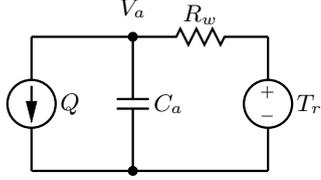

Figure 3: Model A TEC. The components C_a, R_w, Q and T_r respectively represent the lumped thermal mass of the freezer interior, thermal resistance of the envelope, the heat extracted from the freezer interior and the room at constant temperature. V_a is the model output, i.e. the freezer temperature.

4.1.2. Model residuals analysis

Fig. 4 shows the logarithm of the absolute value of Model A residuals autocorrelation function. The logarithm is to allow a clear separation between small values. Checking for autocorrelation in the model residuals is of importance to assess whether the model is able to capture all the dynamics contained in the training data set. This analysis consists in a visual comparison between the autocorrelation functions of model residuals and white noise (uncorrelated by definition). The latter is shown with the dashed line and should be intended as the threshold above which the model residuals are correlated in time. In the case of Model A, residuals are significantly correlated, an evidence that indicates poor model performance.
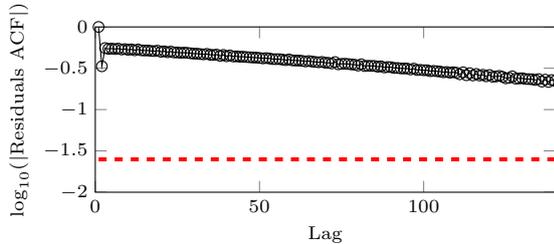

Figure 4: The autocorrelation of Model A residuals (full line) and white noise (dashed line).

4.2. Model B (linear second order)

4.2.1. Model formulation

From the measurements, it was possible to observe a time delay between the activation of the freezer compressor and initial temperature decay. This is because the thermal inertia of the freezer cold heat exchanger, that needs to cool down before being able to extract heat from the freezer interior. To account for such an effect, Model B has an additional RC branch with respect to the previous model. From Fig. 5, the new components C_e and R_e respectively represent the thermal mass of the heat exchanger and the thermal contact resistance between the exchanger and the rest of the freezer cold mass. The state and input vectors of Model B are as

$$\boldsymbol{x}^T = \begin{bmatrix} V_a & V_e \end{bmatrix}$$
$$\boldsymbol{u}^T = \begin{bmatrix} T_r & P \end{bmatrix}, \quad (20)$$

while the stochastic state space matrices are:

$$A = \begin{bmatrix} -\frac{1}{C_a R_w} - \frac{1}{C_a R_e} & \frac{1}{C_a R_e} \\ \frac{1}{C_e R_e} & -\frac{1}{C_e R_e} \end{bmatrix} \quad (21)$$

$$B = \begin{bmatrix} \frac{1}{C_a R_w} & 0 \\ 0 & -\frac{\text{COP}}{C_e} \end{bmatrix} \quad (22)$$

$$W = \text{diag}(w_0, w_1) \quad (23)$$

$$C = \begin{bmatrix} 1 & 0 \end{bmatrix} \quad (24)$$

where $\text{diag}(\cdot)$ denotes the diagonal matrix with elements as in the argument list. The values of the estimated parameters are shown in Table A.7.
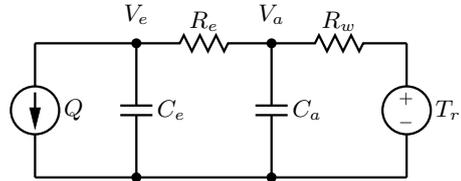

Figure 5: Model B TEC. The additional RC branch decouples between the thermal masses of the freezer interior and heat exchanger.

4.2.2. Model identification and validation

As visible from Fig. 6, Model B residuals are significantly less correlated than in the previous

case. This indicates that the additional state absorbed a part of the dynamics that were left unexplained by the previous model. We now apply the procedure described in 3.6 to validate the model extension. The deviance (10) calculated using the log-likelihood values in Table A.6 and A.7 is $D = 10665$. The p-value (13) of the current model extension is very close to zero, indeed below the 5% threshold. The null hypothesis is therefore rejected and Model B is considered a valid model.
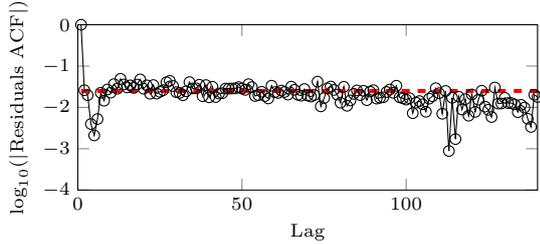

Figure 6: The autocorrelation of Model B residuals (full line) and white noise (dashed line).

4.3. Model C (linear third order)

4.3.1. Model formulation

As shown in Fig. 7 and with respect to the previous model, an additional state C_w is added to decouple between the thermal masses of the freezer envelope and air content. The resistor R_a models the thermal resistance between the two. Model C state and input vectors are

$$
\begin{aligned}
\boldsymbol{x}^T &= \begin{bmatrix} V_e & V_a & V_w \end{bmatrix} \\
\boldsymbol{u}^T &= \begin{bmatrix} T_r & P \end{bmatrix},
\end{aligned}
\tag{25}
$$

while the stochastic state space matrices are as:

$$
A = \begin{bmatrix}
\frac{-1}{C_e R_e} & \frac{1}{C_e R_e} & 0 \\
\frac{1}{C_a R_e} & \frac{-1}{C_a R_a} + \frac{-1}{C_a R_e} & \frac{1}{C_a R_a} \\
0 & \frac{1}{C_w R_a} & \frac{-1}{C_w R_w} + \frac{-1}{C_w R_a}
\end{bmatrix}
\tag{26}
$$

$$
B = \begin{bmatrix}
0 & -\frac{\text{COP}}{C_e} \\
0 & 0 \\
\frac{1}{C_w R_w} & 0
\end{bmatrix}
\tag{27}
$$

$$
W = \text{diag}(w_0, w_1, w_2)
\tag{28}
$$

$$
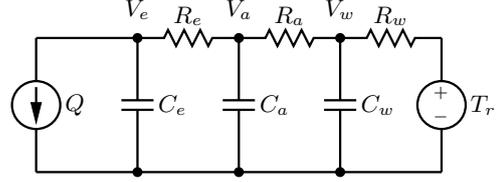C = \begin{bmatrix} 0 & 1 & 0 \end{bmatrix}
\tag{29}
$$

Figure 7: Model C TEC. The freezer interior thermal mass is further decoupled by adding another RC branch.

4.3.2. Model identification and validation

The autocorrelation of Model C residuals in Fig. 8 further improved with respect to the previous models, and only a few points are above the autocorrelation threshold. The deviance of the current model extension is $D = 7.0$. The associated p-value is 3.0%, that is below the 5% significance level. The null hypothesis is rejected and Model C is considered a valid model.
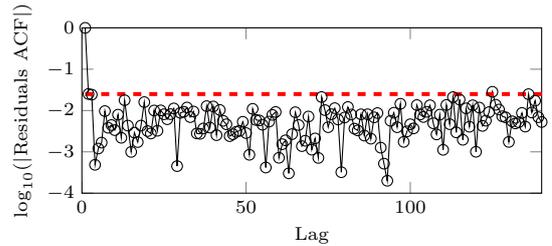
Figure 8: The autocorrelation of Model C residuals (full line) and white noise (dashed line).

4.4. Model D (linear fourth order)

4.4.1. Model formulation

As visible from Fig. 9 and in comparison with Model C, an additional RC branch further decouples between freezer thermal masses. The complete formulation and the model residuals analysis are skipped because, as shown in the following paragraph, the model extension is not significant.
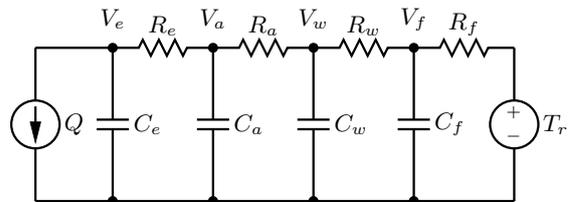
Figure 9: Model D TEC.

4.4.2. Model validation

The deviance of the current model extension is $D = 1.0$, that originates a p-value of 61%. As the p-value is well above the 5% threshold, the null hypothesis cannot be rejected and the model extension is not valid.

4.5. Model E (nonlinear third order)

4.5.1. Model formulation

As known, the COP of an ideal refrigeration cycle is given by the reversed Carnot cycle formula:

$$\mathrm{COP_{ideal}}(T_H, T_C) = \frac{T_C + 273}{T_H - T_C}, \qquad (30)$$

where T_H and T_C are the temperatures in °C of the hot and cold heat reservoir, respectively. In other words, the refrigeration cycle ability to extract heat depends on the temperature difference with the exterior. This effect was not considered in the previous linear models, where the COP was modelled as a constant coefficient. Model E is a third order model as Model C where the heat extracted from the freezer chamber is described by:

$$Q = P \cdot \eta \cdot \mathrm{COP_{ideal}}(T_r, V_e), \qquad (31)$$

where η can be regarded to as the efficiency of the implemented refrigeration cycle with respect to the ideal case, and the hot and cold heat reservoirs are approximated with the room and freezer cold side temperature. With reference to the stochastic state space representation (1)-(2), the complete formulation of Model E is as:

$$\boldsymbol{x}^T = \begin{bmatrix} V_e & V_a & V_w \end{bmatrix} \qquad (32)$$

$$\boldsymbol{u}^T = \begin{bmatrix} T_r & P\dfrac{V_e + 273}{T_r - V_e} \end{bmatrix} \qquad (33)$$

$$A = \begin{bmatrix} \frac{-1}{C_e R_e} & \frac{1}{C_e R_e} & 0 \\ \frac{1}{C_a R_e} & \frac{-1}{C_a R_a} + \frac{-1}{C_a R_e} & \frac{1}{C_a R_a} \\ 0 & \frac{1}{C_w R_a} & \frac{-1}{C_w R_w} + \frac{-1}{C_w R_a} \end{bmatrix} \qquad (34)$$

$$B = \begin{bmatrix} 0 & -\frac{\eta}{C_e} \\ 0 & 0 \\ \frac{1}{C_w R_w} & 0 \end{bmatrix} \qquad (35)$$

$$W = \mathrm{diag}(w_0, w_1, w_2) \qquad (36)$$

$$C = \begin{bmatrix} 0 & 1 & 0 \end{bmatrix} \qquad (37)$$

that is nonlinear as the input (33) depends on a component of the state vector.

4.5.2. Model identification and validation

The autocorrelation of the model residuals is shown in Fig. 10 and has a similar behavior as for Model C. Again, only a few components of the autocorrelation function are above the dotted line, thus indicating a good overall capacity of Model E to describe the dynamics contained in the training data set. The deviance test is not computed because Model E is not an extension of the previous, rather it relies on a different mathematical description of the refrigeration process. Nevertheless, it is worth noting than Model E has a better fitting than Model C because, although the two have same number of parameters, Model E achieves a larger log-likelihood value.
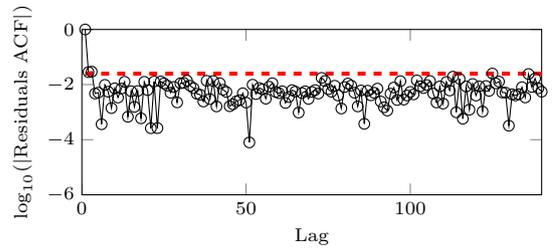

Figure 10: The autocorrelation of Model E residuals (full line) and white noise (dashed line).

5. An empirical estimation of the freezer components thermal characteristics

In this section, we perform a purely empirical estimation of the physical values of the main freezer components. This process should not be meant as a replacement of the previous grey-box modelling methodology, that is in fact a more general and powerful tool as parameters are estimated from measurements, regardless of unknown or approximative information on the physical characteristics of the freezer components. Moreover, grey-box models have the advantage of being tuned on the specific device to model, a degree of freedom that is not achievable by first principles based models. Nevertheless, the analysis proposed in this section is of importance to verify whether the previously identified parameters are of reasonable order of magnitude and if the circuit components absorbed those dynamics they were designed for. The estimated physical characteristics of the main freezer components are in Table 1. The thermal capacities are

calculated as

$$C = M \cdot c, \qquad (38)$$

where M, c respectively denote a mass (calculated as a volume times the density of the component) and specific heat capacity. Volumes are estimated by measuring the size of the components. In the case of a non-accessible part, the size was reasonably guessed. The thermal resistance of the isolation layer is computed as

$$R = \frac{1}{\lambda} \cdot \frac{t}{S} \qquad (39)$$

where λ, t, S respectively denote the thermal conductivity, thickness and lateral surface of the freezer envelope. Discrepancies can be noted when comparing the values in Table 1 with the fitted model parameters. For example, in the case of Model E, the value of C_a is approximately 2 orders of magnitude larger than the empirically calculated thermal capacity of the air, and vice-versa in the case of C_e and the thermal capacity of the heat exchanger. This indicates that the capacitors of Model E did not absorbed those dynamics for which it was originally thought. Rather, C_a is a lumped description of the thermal mass of several freezer parts. In spite of this, the total values of the best fitting models thermal capacity and resistance are with same order of magnitude as the global empirical, an indication that the found values of the models parameters are globally meaningful.

Table 1: Physical properties and empirically estimated characteristics of the freezer main components.

Component	Chamber	Isolation Layer	Heat Exchanger
Material	Air	Polyurethane foam [15]	Aluminium
Specific heat capacity c ($\mathrm{J\,kg^{-1}\,K^{-1}}$)	1000	1500	897
Total mass M (kg)	0.5	8	10
Thermal capacity C ($\mathrm{J\,K^{-1}}$)	5×10^2	5×10^3	1×10^4
Thermal conductivity λ ($\mathrm{W\,m^{-1}\,K^{-1}}$)	–	0.025	–
Thickness t (m)	–	0.08	–
Lateral surface S ($\mathrm{m^2}$)	–	2.4	–
Thermal resistance R ($\mathrm{K\,W^{-1}}$)	–	1.3	–

6. Models Performance Assessment

Table 2 shows, for each identified model, the mean and standard deviation of the model residuals derived from 20-minute-ahead predictions using a validation data set. The best performing model (i.e. smallest residuals bias and standard deviation) is Model E, while Model A is the worst, thus overall confirming the model identification results. Moreover, Model D does not show better performance than Model C, therefore validating the outcome of the previous inference analysis according to which the extension to a fourth order linear model was not statistically significant.

Table 2: Model residuals statistics for 20-minute ahead predictions with a PRBS validation data set.

Model	$\bar{e}$ [°C]	σ_e [°C]
Model A	0.593	2.8
Model B	0.227	0.91
Model C	0.106	0.60
Model D	0.145	0.74
Model E	0.044	0.45

Table 3 shows the same statistical analysis as in the previous table, but performed with a validation data set measured under conventional thermostatic control for the purpose of highlighting the prediction performance of the models during conventional operation. Overall, the prediction performance of the models in increased. This could be explained by the fact that under thermostatic regime, the temperature of the freezer varies in a smaller range than in the PRBS case, therefore possible nonlinear effects due to temperature variations not explained in the models are reduced.

Table 3: Model residuals statistics for 20-minute ahead predictions under conventional thermostatic regime.

Model	$\bar{e}$ [°C]	σ_e [°C]
Model B	0.15	0.73
Model C	0.056	0.29
Model E	0.023	0.27

7. Optimizing the power consumption of a freezer using model predictive control

7.1. Introduction and objective

A paradigm often advocated in the existing literature to increase the proportion of electricity production from renewables is to restore an adequate

level of controllability by giving the possibility of shifting the consumption of DSRs [16–20]. Electric heating systems, water heaters and refrigeration units are all loads that, although with different levels of flexibility, can be controlled to temporarily defer the consumption thanks to the their thermal mass. Among several algorithms for shifting the consumption of flexible demand, MPC comes to prominence as a method to achieve the non disruptive controllability of individual DSRs through a consumption incentive signal, like for example a dynamic electricity price [21, 22] or according to the availability of renewable production, as done in [23, 24]. MPC consists in determining the electrical power consumption trajectory of a DSR that minimizes a given penalty function (like the total cost of the operation) while obeying to consumer comfort and operational constraints by implementing a DSR prediction model.

In this section, we describe an experimental application of MPC to achieve a shift in the consumption of the previously described instrumented freezer. The MPC experiments are carried out implementing several of the freezer presented in Section 4, with the main objective being to assess their performance in a practical application.

7.2. MPC general formulation

The MPC strategy is formulated and actuated at discrete time intervals of duration T_s. The index i denotes the rolling time interval, while k is a generic discrete time index. The freezer temperature prediction models, which were formulated in continuous time, are also discretized as shown in Appendix B. The objective of the MPC formulation is to determine the sequence $\boldsymbol{P}_i^o = \begin{bmatrix} P_i^o & P_{i+1}^o & \cdots & P_{i+N}^o \end{bmatrix} \in \mathbb{R}^{N+1}$, i.e. the freezer power consumption from the current time instant and for the next N. The formulation consists of the following optimization problem:

$$\boldsymbol{P}_i^o = \underset{\boldsymbol{P}_i \in \mathcal{P}}{\arg \min} \sum_{k=i}^{i+N} P_k \cdot c_k \qquad (40)$$

subject to:

$$\overline{T}_{k+1} = f(T_k, P_k, T_{r,i}), \quad k = i, \ldots, i+N \quad (41)$$

$$T_{\min} \leq \overline{T}_{k+1} \leq T_{\max}, \quad k = i, \ldots, i+N \quad (42)$$

$$0 \leq P_k \leq P_{\max}, \quad k = i, \ldots, i+N, \quad (43)$$

where $f(\cdot)$ denotes a discrete time freezer model, $\overline{T}$ is the expected value of the temperature prediction, $T_{\min}$, $T_{\max}$ define the range where the freezer temperature is allowed, and $P_{\max}$ is the maximum power consumption of the freezer. As shown in Appendix B, freezer linear models originate convex optimization problems because the inequality in (42) can be written as a linear function of the decision vector. As known, convexity is an appealing property for optimization problems because it is a sufficient condition for the uniqueness of the solution. Said otherwise, if a solution to the problem exists, it is the global optimum. Moreover, there exist efficient algorithms to solve convex optimization problems. On the contrary, the optimization problem of the MPC with the nonlinear freezer model is nonconvex. This aspect will be further addressed when presenting the experimental results. Said in words, the optimization problem in (40)-(43) seeks for the freezer power consumption trajectory that minimizes the penalty function while respecting the following operational constraints:

- keeping an adequate temperature level to preserve food quality according to the consumer preferences. According to food storage regulation [25, 26], freezer temperature should be regulated at $-18\,^\circ\mathrm{C}$, although temperatures in the range from -22 to $-28\,^\circ\mathrm{C}$ are indicated to achieve longer storage periods. In this case, the temperature bounds are chosen as $T_{\min} = -27\,^\circ\mathrm{C}$ and $T_{\max} = -18\,^\circ\mathrm{C}$.

- the freezer power consumption during the on phase of the compressor is modelled as a constant term, and it is limited by the maximum power absorption of the freezer, roughly $68\,\mathrm{W}$. We recall from Section 2 that the compressor can be only on-off controlled. Therefore, we use the following procedure to turn the real scalar power consumption set-points of (40) into a sequence of on/off pulses of period T_s:

$$\tau_{\mathrm{on},k} = \frac{P_k}{P_{\max}} T_s, \quad k = i, \cdots, i+N \qquad (44)$$

where τ_{on} is the duration in second of the *on* phase. In other words, Eq. (44) performs a pulse width modulation (PWM) to translate the MPC power set-point into an on-off signal that, over the period T_s, delivers an equal amount of electricity. The ratio $\tau_{\mathrm{on},k}/T_s$ is said duty cycle. This formulation is convenient be-

cause it does not require to formulate the optimization problem as a mixed integer programming problem.

The sequence $c_i, \ldots, c_N$ in (40) is a virtual electricity price that must be known in advance for the whole length of the optimization period. In this case, it is chosen as a step signal to allow for evaluating the amount of freezer consumption that the MPC can shift in view of an increase in the electricity price. The constant coefficient N in (40) determines the length of the look-ahead horizon. The electricity that can be virtually stored in the freezer is given by the amount of consumption that is shifted while respecting the temperature constraints. Therefore, N should be chosen larger than the time that the freezer temperature takes to go from the upper to the lower bound or, in other words, larger than the time required to saturate the storage capacity. As highlighted in [27, p. 36], it is worth noting that the formulation (40)-(43) does not react to stepwise decreases of the price signal. In the case such a functionality is of interest, one should considered to implement a quadratic cost function to penalize deviation from a given temperature set-point.
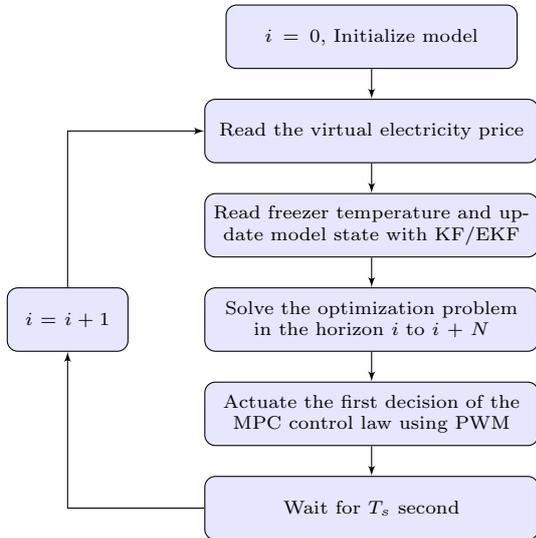

Figure 11: Flow chart of the MPC experiment illustrating the receding horizon policy.

7.3. On the actuation of the MPC law

As is usually the case, the MPC action is actuated in a receding horizon way, meaning that, at each time interval, the state vector of the prediction model is updated using the last available measurements from the freezer, the optimization problem is solved and the first portion of the MPC control law is applied. A diagram summarizing the complete sequence of events performed during the experiments is shown in Fig. 11. At the initial stage, the prediction model is initialized with the latest freezer temperature measurement (steady state conditions are assumed). Then, at each iteration of the receding horizon cycle, the virtual electricity price for the next N periods is acquired, as well as the current temperature measurement. The latter information is used to update the state of the prediction model by a using a Kalman filter (KF). The prediction stage of the KF consists in determining the model state and covariance matrix evolution as:

$$\widehat{\boldsymbol{x}}_{k|k-1} = A_d \widehat{\boldsymbol{x}}_{k-1|k-1} + B_d \boldsymbol{u}_{k-1} \qquad (45)$$

$$P_{k|k-1} = A_d P_{k-1|k-1} A_d^T + WW^T, \qquad (46)$$

where A_d, B_d are the linear discrete state space model matrices (derived in Appendix B), C is the output vector and W is the noise process matrix determined in the parameters estimation process. The Kalman gain is

$$K = P_{k|k-1} C^T \left(C P_{k|k-1} C^T + v^2 \right)^{-1}, \qquad (47)$$

where v is the measurement noise (also known from the parameters estimation). Once the new measurement y_k is available, the state prediction is updated as:

$$\widehat{\boldsymbol{x}}_{k|k} = \widehat{\boldsymbol{x}}_{k|k-1} + K_k(y_k - C\widehat{\boldsymbol{x}}_{k|k-1}) \qquad (48)$$

$$P_{k|k} = \left(P_{k|k-1}^{-1} + C^T v^{-1} C \right)^{-1}. \qquad (49)$$

Instead, in the case of Model E, the extended Kalman filter is used. The state prediction is performed as:

$$\widehat{\boldsymbol{x}}_{k|k-1} = f(\widehat{\boldsymbol{x}}_{k|k}, P_i, T_{r,i}) \qquad (50)$$

using the discretized version of the nonlinear model in (32)-(37). The state covariance matrix, KF gain and update steps are performed using the equations (46)-(49) as in the previous case, but A_d is now as:

$$A_d = \left. \frac{\partial f}{\partial \boldsymbol{x}} \right|_{x_{k-1|k-1}, u_{k-1}}, \qquad (51)$$

namely the first order Taylor expansion of the model with respect to the state vector. Finally from

Fig. 11, once the model is updated, the optimization problem is solved in order to determine the optimal control law $\boldsymbol{P}_i^o$. Then, the decision P_i^o for the current instant of time is extracted and actuated in the PWM sense (Eq. (44)) by regulating the on-off timing of the controllable freezer power plug. A further consideration concerns the implementation of temperature soft constraints in the optimization problem. In fact, in the formulation (40)-(43), the freezer temperature is strictly allowed only in a well determined range. If the temperature hard constraint (42) is not satisfied (for example at the time instant $i + 1$ because unmodelled system dynamics, noise or consumer behavior), the optimization problem is unfeasible, causing a failure of the control system. It is therefore convenient to implement a sequence of positive slack variables $\boldsymbol{s} \in \mathbb{R}^{N+1}$ to relax the constraints, as:

$$\{\boldsymbol{P}_i^o, \boldsymbol{s}_i^o\} = \underset{\{\boldsymbol{P}_i, \boldsymbol{s}_i\} \in \Omega}{\arg \min} \left(\sum_{k=i}^{N} P_k \cdot c_k + b_k \cdot s_k \right) \quad (52)$$

subject to:

$$\overline{T}_{k+1} = f(T_k, P_k, T_{r,i}), \quad k = i, \ldots, i+N \quad (53)$$

$$\widehat{T}_{k+1} \leq T_{\max} + s_k, \quad k = i, \ldots, i+N \quad (54)$$

$$\widehat{T}_{k+1} \geq T_{\min} - s_k \quad k = i, \ldots, i+N \quad (55)$$

$$s_k \geq 0 \quad k = i, \ldots, i+N \quad (56)$$

$$0 \leq P_k \leq P_{\max}, \quad k = i, \ldots, i+N, \quad (57)$$

where b_k, $k = i+1, \ldots, i+N$ are coefficients that should be chosen much larger than c_k. In this way, deviations from the optimal temperature range are allowed but not convenient because they are strongly penalized in the cost function. A final aspect regards the actuation of the PWM signal and the on/off transitions of the freezer, which are of concern as can affect the lifetime of the compressor relay. Although no explicit policy for limiting the number of transitions was formulated in the MPC, we put in place the following two mechanisms to reduce it:

- each second cycle of the PWM control signal is horizontally flipped, as depicted in Fig. 12. This allows to reduce from 2 to 1 the number of transitions per cycle;

- on or off PWM pulses with duration shorter than 10 second are ignored. For example, if a given PWM period has a duty cycle shorter than 10 s, the cycle is considered as it was fully off, and vice-versa.

Since the PWM and transformations described above, the control trajectory that is finally actuated is an approximation of the original MPC law. This might lead to violate the temperature constraints during the actuation period that, however, can be chosen small enough to make them negligible. Eventual prediction and actuation errors are absorbed by the receding horizon formulation and are taken into account in the following actuation period. Another source of error that impacts the optimality of the actuated control law is the non null computation time required to solve the optimization problem. In fact, while the solver is computing the freezer state is left unaltered with respect to the previous receding horizon cycle; as the length of the receding horizon cycle (T_s, 120 s) must be hardly met, the correct timing of the PWM cycle is compromised, especially if the computation time extends for too long. For example, considering the freezer on from the previous cycle, a computation time of 20 s and $\tau_{\mathrm{on},k} = 0$ s, the finally actuated duty cycle would be 0.16 instead of 0.
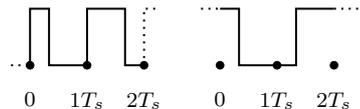

Figure 12: The PWM signal before (left) and after (right) flipping horizontally the second cycle of the period. This allows to halve the total number of on/off transitions.

7.4. MPC experimental results

This section presents the results of a consumption shifting experiment using a MPC-controlled domestic freezer. The objective of the experiment is to assess in practice the performance of the power-to-temperature freezer prediction models, thereby addressing the model selection process also from the application perspective. We compare the performance of three different predictions models, namely Model B, Model C and Model E. The three resulting MPC setups are respectively referred to as MPC-B, MPC-C and MPC-E. The sample time T_s is 120 s, and N is 270, that corresponds to an optimization horizon length of 5 hour. Each MPC experiment lasts for 6 hours. As for the identification experiments, consumer behavior is not considered, i.e. the freezer content stays unchanged and the door is closed. To assure equal conditions during the experiments, the room temperature was regulated to $23\,^\circ\mathrm{C}$.
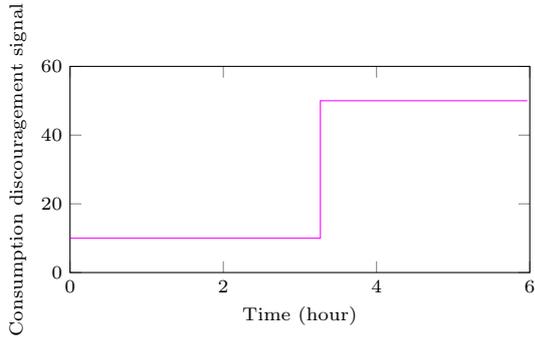
Figure 13: The virtual electricity price.

Figure 14: The MPC-C power consumption control law and the actuated freezer power consumption averaged on a 2 minute interval.

Figure 15: The real-time freezer power consumption (sampled at 10 s) and the average on a 2 minute interval during a portion of the MPC-C experiment.

Figure 16: The freezer temperature during the three MPC experiments. The horizontal dashed line denotes the temperature constraints, while the continuous vertical line indicates the instant of time when the large value of the virtual electricity price is released.

The virtual electricity price (implemented in the MPC cost function by the sequence c_k, $k = i, \ldots, i + N$) is shown in Fig. 13. Considering the MPC formulation (i.e. penalty function linear in the consumption and freezer temperature allowed in a given range), the expected behavior is that the freezer will reach the lowest allowed temperature before the larger value of c_k in order to decrease as much as possible the consumption of expensive electricity. Fig. 14 compares the receding horizon power consumption trajectory as determined by the MPC and the actuated freezer power consumption averaged on a 120 second interval. The difference between the two profiles is due to the fact that the freezer consumption is, as mentioned in Section 7.2, modelled as a constant term, while in the real case it depends on the absorption of the induction motor. Fig. 15 shows the freezer power consumption measurements (at 10 s resolution) and the respective average calculated on a 120 second time interval. In the former profile, the effect of the PWM is evident. Fig. 16 shows the freezer temperature as measured during the experiments. As visible, MPC-C is close to reach the lowest temperature ($-26.53\,°C$ while the limit is $-27\,°C$) just before the release of the large virtual electricity price. This evidence indicates that the controller is able to exploit nearly all the storage capacity allowed by the MPC setup.

In order to formally compare the performance of the different MPC setups, we use the following three metrics:

m_0: the value of the MPC cost function (52) evaluated, for each experiment, considering the actuated consumption profile and measured temperature.

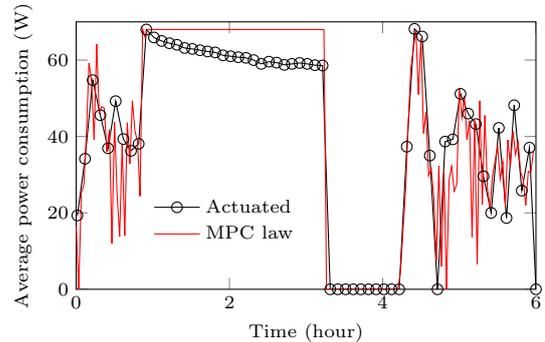m_1: amount of electricity shifted (or virtual storage capacity), evaluated as the nominal power

13

of the freezer times the duration between the instant of time when the larger value of the virtual electricity price is triggered until when the freezer temperature reaches the upper threshold;

m_2: distance from the upper temperature limit when the upper bound constraint is violated on the duration of the experiments in number of discrete time steps L. Formally it is as:

$$m_2 = \sum \frac{1}{L} d_k \qquad (58)$$

where

$$d_k = \begin{cases} 0, & T_k <= T_{max} \\ T_k - T_{max}, & T_k > T_{max} \end{cases}, \qquad (59)$$

for $k = 0, \ldots, L-1$;

m_3: maximum violation of the temperature upper bound constraint (T_{max}).

The metrics calculated for the MPC experiments are summarized in Table 4. The metrics m_0 and m_1 are in favor of MPC-C, meaning that it achieves the lowest cost of operation and largest shift of consumption. As far as the temperature comfort metrics are concerned, the MPC-B achieves the smallest violation of the upper temperature bound constraint (m_3), although MPC-C has the lowest average violation (m_2). Nonlinear Model E, that had the best prediction performance in the previous section, does not perform well in the respective MPC setup. This is to ascribe to the fact that the actuated control law is strongly suboptimal. Even if nonconvex optimization algorithm for global optimum search are available (like PSO or genetic algorithms), they have been not considered because the associated computational burden is relevant. Moreover, considering the experimental results, it can be said that implementing complex nonconvex algorithm is not justified by the performance of the MPC-C that, as discussed while describing Fig. 16, is already able to exploit nearly all the flexibility of the freezer while showing overall a good capability of satisfying freezer constraints. Another solution, that however has not been attempted in the proposed experiments for the same reason explained above, could consists in formulating a convex optimization problem by linearizing nonlinear Model E as similarly done for the state estimation in the extended Kalman filter.

Table 4: Summary of MPC Performance metrics.

Implemented Model	m_0 (cost)	m_1 (Wh)	m_2 (°C)	m_3 (°C)
MPC-B	1.7×10^5	52.1	0.06	0.43
MPC-C	1.5×10^5	74.8	0.04	0.68
MPC-E	2.0×10^5	38.5	0.39	1.29

In addition to the proposed metrics, Table 5 reports the average computation time required to determine the MPC solution (single thread process on an Intel i7 2.10 GHz) and the round trip storage efficiency, calculated as the ratio between the amount of electricity invested to reach the freezer lower temperature and the one that is harvested. As expected, the computation time for linear models is lower than for the nonlinear case, that requires to solve a nonconvex optimization problem. The round trip efficiency of MPC-C is the lowest because, by achieving a lower temperature, thermal losses are increased.

Table 5: Additional performance metrics.

Implemented Model	Computation time (s)	Round trip efficiency
MPC-B	4.5	82%
MPC-C	5.7	51%
MPC-E	21.6	54%

8. Conclusions and perspectives

We described the application of grey-box modelling to identify suitable power consumption-to-temperature models of a domestic refrigeration using experimental measurements from an instrumented 333 liter freezer. Consumer behavior was not considered at this stage. Models were formulated using stochastic differential equations (SDEs) and identified used maximum likelihood estimation (MLE). The proposed models were validated by checking the model residuals correlation, and model extensions were cross-validated to detect model over-fitting. Among the presented linear models, it has been shown that a third order model is able to capture nearly all the dynamics contained in the

measurements. While the extension to a fourth order linear model was not justified by statistical evidence, it was shown that implementing a nonlinear description of the reverse Carnot cycle leads to a marginal improvement of the model prediciton performance. As the modelling effort was framed within the context of intelligent energy strategies for demand side management, the second part of the paper is devoted to assessing the models performance in a demand response experiment. It consisted in quantifying the virtual storage action that a freezer can achieve using model predictive control (MPC) and the prediction models previously identified. From the experiments, it emerged that the third order linear model was able to harvest nearly all the flexibility inherent the freezer operation. Also, it was seen that the mathematical formulation plays in favor of linear models because they result in convex optimization problems that are tractable and efficient to solve. In the best performing experiment, a virtual storage capacity equivalent to 75 Wh of electrical energy with a round trip efficiency of 51% was measured. Although consumer behavior was not considered in the experiments, these figures already give an overview on the amount of storage capacity that is possible to harvest from the freezer operation in an ideal condition. Considering the low specific energy density, further studies should be devoted to asses the cost-benefit of the potential deployment of freezer-based demand response programs. Phase change materials (PCMs), which have been proven to enhance storage capacity [28], should be indeed considered in future identification and MPC experiments. Another challenging aspect regards the identification of consumer behavior (in terms of both additional food load, that might contribute to increase storage performance, and door opening that could cause a quick drop of achieved storage level), that is relevant for estimating the freezer flexibility in a real operating scenario. In this context, the proposed grey-box freezer models could be used as a backbone where to plug models of the consumer behavior. The latter kind of models might rely on completely different modelling approaches (e.g. pattern recognition techniques) and can use the former as an interface for the physical heat transfer principles. Overall, this strategy would result in a model-based approach and could be compared with model-free techniques (such as in [29]).

Appendix A. Identified Model Parameters

Table A.6: Model A identification summary.

Parameter	Unit	Value	σ
C_a	$\mathrm{J\,K^{-1}}$	2.99×10^3	5.00×10^4
R_w	$\mathrm{K\,W^{-1}}$	5.69×10^{-1}	7.50×10^{-1}
α	$-$	-4.54	7.0×10^{-3}
COP	$-$	3.01×10^{-1}	6.07×10^{-3}
log-likelihood value		19833.1	-

Table A.7: Model B identification summary.

Parameter	Unit	Value	σ
C_a	$\mathrm{J\,K^{-1}}$	9.74×10^3	2.12×10^3
C_e	$\mathrm{J\,K^{-1}}$	2.28×10^3	1.67×10^2
R_e	$\mathrm{K\,W^{-1}}$	9.74×10^{-2}	7.03×10^{-3}
R_w	$\mathrm{K\,W^{-1}}$	9.93×10^{-1}	1.80×10^{-1}
α_0	$-$	-1.36×10^1	2.76
α_1	$-$	-2.59	1.45×10^{-1}
COP	$-$	1.04	1.87×10^{-1}
log-likelihood value		25165.4	$-$

Table A.8: Model C identification summary.

Parameter	Unit	Value	σ
C_a	$\mathrm{J\,K^{-1}}$	4.76×10^3	2.45×10^3
C_e	$\mathrm{J\,K^{-1}}$	1.05×10^3	8.37×10^2
C_w	$\mathrm{J\,K^{-1}}$	8.11×10^3	4.60×10^3
R_a	$\mathrm{K\,W^{-1}}$	4.97×10^{-1}	2.82×10^{-1}
R_e	$\mathrm{K\,W^{-1}}$	1.12×10^{-1}	8.14×10^{-2}
R_w	$\mathrm{K\,W^{-1}}$	1.28	7.20×10^{-1}
α_0	$-$	-8.31	1.7×10^{-2}
α_1	$-$	-6.83	3.8×10^{-2}
α_2	$-$	-3.15	2.6×10^{-1}
COP	$-$	7.68×10^{-1}	1.65×10^{-1}
log-likelihood value		25168.9	$-$

Table A.9: Model D identification summary.

Parameter	Unit	Value	σ
C_a	$\mathrm{J\,K^{-1}}$	1.25×10^4	2.02×10^3
C_e	$\mathrm{J\,K^{-1}}$	1.22×10^3	2.63×10^3
C_w	$\mathrm{J\,K^{-1}}$	5.23×10^3	1.63×10^3
C_f	$\mathrm{J\,K^{-1}}$	3.94×10^3	8.60×10^4
R_a	$\mathrm{K\,W^{-1}}$	4.81×10^{-1}	1.17×10^{-5}
R_e	$\mathrm{K\,W^{-1}}$	1.12×10^{-1}	1.90×10^{-1}
R_w	$\mathrm{K\,W^{-1}}$	6.25×10^{-1}	9.34×10^{-2}
R_f	$\mathrm{K\,W^{-1}}$	1.08	1.92×10^{-1}
η	$-$	5.38×10^{-1}	2.97×10^{-1}
α_0	$-$	-7.20	1.1×10^{-1}
α_1	$-$	-3.66	3.4×10^{-2}
α_2	$-$	-1.1×10^1	2.2×10^{-2}
log-likelihood value		25169.9	$-$

Table A.10: Model E identification summary.

Parameter	Unit	Value	σ
C_a	$\mathrm{J\,K^{-1}}$	1.25×10^4	3.80×10^{-1}
C_e	$\mathrm{J\,K^{-1}}$	1.22×10^3	1.03×10^2
C_w	$\mathrm{J\,K^{-1}}$	8.30×10^3	1.59×10^2
R_a	$\mathrm{K\,W^{-1}}$	1.61×10^{-1}	8.66×10^{-5}
R_e	$\mathrm{K\,W^{-1}}$	1.47×10^{-1}	8.49×10^{-4}
R_w	$\mathrm{K\,W^{-1}}$	6.32×10^{-1}	3.53×10^{-3}
η	$-$	5.67×10^{-1}	2.97×10^{-1}
α_0	$-$	-7.20	1.1×10^{-1}
α_1	$-$	-3.66	3.4×10^{-2}
α_2	$-$	-1.1×10^1	2.2×10^{-2}
log-likelihood value		25187.6	$-$

Appendix B. Formulation of the MPC optimization problem

Freezer linear models

The discretized version of the linear continuous time stochastic state space model (1) is as:

$$\boldsymbol{x}_{i+1} = A_d \boldsymbol{x}_i + B_d \boldsymbol{u}_i + W \omega_i \qquad (B.1)$$

$$A_d = A T_s + \mathbb{I}_{n \times n} \qquad (B.2)$$

$$B_d = B T_s \qquad (B.3)$$

where T_s is the sampling time and the other symbols are as defined in Section 3.3. The observation equation is as in (2). For the moment, we shall assume that $\boldsymbol{u} = P$ and $B \in \mathbb{R}^n$. We will extend to the multi-input case later. The expected value of the vector state for $i = 0$ is as

$$\overline{\boldsymbol{x}}_1 = A_d \overline{\boldsymbol{x}}_0 + B_d P_0. \qquad (B.4)$$

The expected value of the system output at $i = 2$ is

$$\overline{T}_2 = C\big(A_d \overline{\boldsymbol{x}}_1 + B_d P_1\big). \qquad (B.5)$$

Replacing the second last expression in the last yields to:

$$\overline{T}_2 = CA_d\big(A_d \overline{\boldsymbol{x}}_0 + B_d P_0\big) + CB_d P_1. \qquad (B.6)$$

Iterating until the time instant N finally gives:

$$\overline{T}_N = CA_d^N \boldsymbol{x}_0 + CA_d^{N-1} B_d P_0 + \cdots + CB_d P_{N-1}. \qquad (B.7)$$

Denoting the sequences $[\overline{T}_1, \ldots, \overline{T}_N]^T$, $[P_0, \ldots, P_{N-1}]^T$ with $\boldsymbol{T}$ and $\boldsymbol{P}$ respectively, the expression above can be reformulated using the matrix product notation as:

$$\boldsymbol{T} = \Phi \overline{\boldsymbol{x}}_0 + \Theta(B)\boldsymbol{P}, \qquad (B.8)$$

where

$$\Phi = \begin{bmatrix} CA_d & \cdots & CA_d^N \end{bmatrix}^T \qquad (B.9)$$

$$\Theta(B) = \begin{bmatrix} CA_d B_d & 0 & \cdots & 0 \\ \vdots & \vdots & \ddots & \vdots \\ CA_d^N B_d & CA_d^{N-1} B_d & \cdots & CB_d \end{bmatrix}. \qquad (B.10)$$

In the multi-input case with $B_d \in \mathbb{R}^{n \times 2} = [B_{d,0}, \ B_{d,1}]$ and $\boldsymbol{u}^T = [P, \ T_r]$, the expected value of the state vector is as:

$$\overline{\boldsymbol{x}}_{i+1} = A_d \overline{\boldsymbol{x}}_i + B_{d,0} P_i + B_{d,1} T_{r,i} \qquad (B.11)$$

and the system output can be therefore expressed as:

$$\boldsymbol{T} = \Phi \overline{\boldsymbol{x}}_0 + \Theta(B)\boldsymbol{P} + \Theta(E)\boldsymbol{v}, \qquad (B.12)$$

i.e. adding the input and the respective transition matrix $\Theta(E)$. Eq. (B.12) can be used to express the inequality constraints (42). Therefore, the optimization problem (52)-(57) can be finally expressed in a standard form as:

$$\{\boldsymbol{P}^o, \boldsymbol{s}^o\} = \underset{\{\boldsymbol{P},\boldsymbol{s}\} \in \Omega}{\arg\min} \left(\boldsymbol{P}^T \boldsymbol{c} + \boldsymbol{s}^T \boldsymbol{c} \right) \qquad (B.13)$$

subject to:

$$\Phi \overline{\boldsymbol{x}}_0 + \Theta(B)\boldsymbol{P} + \Theta(E)\boldsymbol{v} \leq T_{\max} \qquad (B.14)$$

$$-\Phi \overline{\boldsymbol{x}}_0 - \Theta(B)\boldsymbol{P} - \Theta(E)\boldsymbol{v} \leq -T_{\min} \qquad (B.15)$$

$$\boldsymbol{P} \leq \boldsymbol{P}_{\max} \qquad (B.16)$$

$$-\boldsymbol{P} \leq 0 \qquad (B.17)$$

$$-\boldsymbol{s} \leq 0 \qquad (B.18)$$

that can be solved for example using the *linprog* function in Matlab.

Freezer nonlinear model

The discretized version of the nonlinear model is obtained in the same way as for the linear models. However, in this case the coefficient B_d will depend on the state variable. When iterating the time expansion as previously done to determine (B.8), the temperature evolution cannot be expressed anymore as a linear function of the decision vector $\boldsymbol{P}$, thus originating a nonconvex optimization problem. The final problem is formulated as in (52)-(57) and solved using the Matlab function *fmincon*.

Acknowledgement

References

1. Annual energy outlook 2012. Tech. Rep.; US Energy Information Administration; 2012.
2. Xydis G. Wind energy to thermal and cold storage—a systems approach. *Energy and Buildings* 2013;56:41–7.
3. Douglass P, Garcia-Valle R, Nyeng P, Ostergaard J, Togeby M. Smart demand for frequency regulation: Experimental results. *IEEE Transactions on Smart Grid,* 2013;4(3):1713–20. doi:10.1109/TSG.2013.2259510.
4. Christakou K, Tomozei DC, Le Boudec JY, Paolone M. Gecn: Primary voltage control for active distribution networks via real-time demand-response. *IEEE Transactions on Smart Grid* 2013;PP(99).
5. Hovgaard TG, Larsen LF, Edlund K, Jørgensen JB. Model predictive control technologies for efficient and flexible power consumption in refrigeration systems. *Energy* 2012;44:105–16.
6. Hovgaard TG, Boyd S, Larsen LF, Jørgensen JB. Nonconvex model predictive control for commercial refrigeration. *International Journal of Control* 2013;86:1349–66.
7. Hermes CJ, Melo C, Knabben FT, Gonçalves JM. Prediction of the energy consumption of household refrigerators and freezers via steady-state simulation. *Applied Energy* 2009;86(7).
8. Hermes CJ, Melo C. Assessment of the energy performance of household refrigerators via dynamic simulation. *Applied Thermal Engineering* 2009;29(5).
9. Hovgaard T, Larsen LFS, Skovrup M, Bagterp Jørgensen J. Power consumption in refrigeration systems-modeling for optimization. In: *Advanced Control of Industrial Processes (ADCONIP), 2011 International Symposium on*. 2011:234–9.
10. Costanzo GT, Sossan F, Marinelli M, Bacher P, Madsen H. Grey-box modeling for system identification of household refrigerators: A step toward smart appliances. In: *IEEE International Youth Conference on Energy (IYCE)*. 2013:.
11. Juhl R, Kristensen NR, Bacher P, Kloppenborg J, Madsen H. CTSM-R User Guide 2013;.
12. Kristensen N, Madsen H, Jørgensen S. Parameter estimation in stochastic grey-box models. *Automatica* 2004;40(2):225–37. doi:10.1016/j.automatica.2003.10.001.
13. Juhl R, Kristensen NR, Bacher P, Kloppenborg J, Madsen H. Simple example of grey-box modeling of the heat dynamics of a wall with CTSM-R. Tech. Rep.; DTU Compute; 2013.
14. Madsen H, Thyregod P. Introduction to General and Generalized Linear Models. Chapman & Hall/CRC Texts in Statistical Science Series; Chapman & Hall/CRC; 2011.
15. Thermal insulation materials made of rigid polyurethane foam. Tech. Rep.; Federation of European Rigid Polyurethane Foam; 2006.
16. Herter K, Wayland S. Residential response to critical-peak pricing of electricity: California evidence. *Energy* 2010;35:1561–7.
17. Zarnikau JW. Demand participation in the restructured electric reliability council of texas market. *Energy* 2010;35:1536–43.
18. Cappers P, Goldman C, Kathan D. Demand response in u.s. electricity markets: Empirical evidence. *Energy* 2010;35:1526–35.
19. Keane A, Tuohy A, Meibom P, Denny E, Flynn D, Mullane A, O'Malley M. Demand side resource operation on the irish power system with high wind power penetration. *Energy Policy* 2011;39(5):2925–34.
20. Hedegaard K, Ravn H, Juul N, Meibom P. Effects of electric vehicles on power systems in northern europe. *Energy* 2012;48(1):356 –68.
21. Halvgaard R, Poulsen NK, Madsen H, Jørgensen JB. Economic model predictive control for building climate control in a smart grid. In: *IEEE International Conference on Innovative Smart Grid Technologies (ISGT)*. 2012:.
22. Zong Y, Kullmann D, Thavlov A, Gehrke O, Bindner H. Active load management in an intelligent building using model predictive control strategy. In: *IEEE PowerTech*. 2011:.
23. Sossan F, Kosek AM, Martinenas S, Marinelli M, Bindner HW. Scheduling of domestic water heater power demand for maximizing PV self-consumption using model predictive control. In: *IEEE International Conference on Innovative Smart Grid Technologies (ISGT)*. 2013:.
24. Callaway DS. Tapping the energy storage potential in electric loads to deliver load following and regulation, with application to wind energy. *Energy Conversion and Management* 2009;50(5).
25. Are you storing food safely? Tech. Rep.; US Food and Drug Administration; 2015. URL: http://goo.gl/7cScJf.
26. Guidance on Temperature Control Legislation in the United Kingdom. Tech. Rep.; Food Standards Agency; 2007. URL: https://goo.gl/cNxMmI.
27. Sossan F. Indirect control of flexible demand for power system applications. Ph.D. thesis, http://goo.gl/CjnugK; Technical University of Denmark, Department of Electrical Engineering; 2014.
28. Taneja J, Lutz K, Culler D. The impact of flexible loads in increasingly renewable grids. In: *Smart Grid Communications (SmartGridComm), 2013 IEEE International Conference on*. IEEE; 2013:265–70.
29. Ruelens F, Iacovella S, Claessens BJ, Belmans R. Learning agent for a heat-pump thermostat with a set-back strategy using model-free reinforcement learning. *CoRR* 2015;abs/1506.01054. URL: http://arxiv.org/abs/1506.01054.